Desalination and Water Treatment
www.deswater.com
doi: 10.5004/dwt.2019.24137

157 (2019) 157–164
July

Y/Fe/TiO_2 co-doped nano carbon composite for the photocatalytic applications

V. Priya[a], S.K. Krishna[a], V. Sivakumar[b], P. Sivakumar[c,*]

[a]*Department of Chemistry, Chikkaiah Naicker College, Erode 638004, TN, India, emails: priyavelusamy.m.sc@gmail.com (V. Priya), ragul2022@gmail.com (S.K. Krishna)*
[b]*Department of Chemistry, Sri Vasavi College, Erode 638316, TN, India, email: cvabavani@gmail.com*
[c]*Department of Chemistry, Arignar Anna Govt Arts College, Namakkal 637002, TN, India, email: shivagobi@yahoo.com*

Received 13 August 2018; Accepted 20 March 2019

ABSTRACT

A multi-metal catalyst synthesized from *Alternanthera sessilis* is used for the synthesis of nano carbon sphere (NCS) with an average diameter of 50–80 nm. The presence of poly aromatic hydrocarbons favored the formation of fullerene-like carbon balls during the carbon formation. A composite photocatalyst is prepared by co-doping Y/Fe/TiO_2 onto NCS. The synthesized composite catalyst is characterized using X-ray diffraction, scanning electron microscope, energy dispersive X-ray spectroscopy, transmission electron microscope (TEM) and UV–DRS analysis. The TEM image proved the presence of lattice fringes with about 4–5 graphitic layers in 2 nm range, which confirms the graphitic carbon having an interlayer distance of 0.4–0.6 nm. The band gap of TiO_2 showed a considerable reduction in the co-doped carbon composite with an optical band gap of 2.73 eV. The photocatalytic degradation of an anionic azo dye Direct Blue 71(DB71) is evaluated and the composite catalyst is capable of degrading more dye molecules under visible light when compared with that of UV irradiation.

Keywords: Alternanthera sessilis; Waste engine oil; Carbon balls; Direct Blue 71; Band gap

1. Introduction

The upward trend in the population size is expected to continue with roughly 83 million people being added to the world's population every year [1]. This exponential growth in human population increases the urban activities and leads to deforestation, water and air pollution. When the contamination of anthropogenic remains in aquatic resources exceeds the range of local baseline concentration limits, it shall pose threats to environmental sustainability. The irreversible damages to the water bodies make serious threats not only to aquatic ecosystem but also to the terrestrial ecosystem. Even though many advanced technologies are available to treat the waste water, the researchers at present are focusing on a clean and green technology which will minimize the risk of hazardous byproducts. Also, the technologies at present have certain limitations to treat wastewater containing many varieties of pollutants. Photocatalytic decomposition of organic wastes using semiconductor photocatalytic materials has received good attention from researchers owing to its efficiency and generation of lesser byproducts [2]. Among the photocatalysts, TiO_2 has many advantages such as nontoxicity, low cost, extended life time of the photogenerated carriers and long-term stability [3,4]. Whereas, the scope for the large-scale industrial applications of TiO_2 is limited as the band gap of anatase form of TiO_2 is 3.2 eV corresponding to the cut off wavelength of about 390 nm, which can harvest only 3%–4% of the solar energy [5]. In the present context, the usage of UV light for the photocatalysis is not economically viable. Therefore, it is essential to find a visible active photocatalyst that can be conveniently used under freely available solar radiation.

Doping of other suitable materials with TiO_2 can effectively reduce the band gap and thereby the activity of the composite catalyst can be moved to higher wavelength [6]. The red shift in the absorption wavelength makes the

* Corresponding author.

composite catalyst active under the entire visible spectrum which can harness the entire solar radiation. Earlier researchers have demonstrated that doping TiO_2 with some inner transition metal oxides can effectively reduce the energy gap between the valence band and the conduction band and there by TiO_2 can induce the photocatalytic activity under visible light [7–11]. Yttrium (Y) is one of the rare earth metals, which on doping with TiO_2 showed a great improvement in the photocatalytic activity when compared with pure TiO_2 owing to the prevention of electron–hole recombination [12]. Doping of Y with TiO_2 can reduce the band gap, but still there is a plenty of scope available to extend the life of photo excitons. One way of extending the life of photo excitons is doping the Y/TiO_2 composite onto the highly active carbon surface [13]. Murugesan et al. [13] have reported that the nano carbon hollow spheres with a mean size of 40–70 nm on doping with La was observed to effectively decompose methylene blue dye under solar light irradiation. The usage of nano carbon materials for the adsorptive removal of pollutants is most suitable due to the high surface area, whereas it has some limitations such as floating on the surface of water and easy leaching with water owing to their small size and low density. The recovery of the spent composite material can be improved by doping with some magnetically active nano materials such as Fe, Ni oxides. In this work, we have reported the synthesis of nano carbon balls using waste engine oil and the stems of *Alternanthera sessilis*. The Y/Fe/TiO_2 composite was co-doped onto the nano carbon balls and then the resultant Y/Fe/TiO_2@NCS (nano carbon sphere) was analyzed for its ability toward the adsorption and photodecomposition of widely used textile dye Direct Blue 71.

2. Materials and methods

2.1. Materials

All the chemicals used were of analytical grade, purchased and used without further purification. All solutions were made using double distilled water. Waste engine oil that contains mainly Paraffinic-napthanic, Aromatic group (I to IV) and Resinous compounds [14] was used in the preparation of carbon ball.

2.2. Preparation of green catalyst

The muti-metal catalyst was synthesized in a green procedure using the following steps:

2.2.1. Preparation of carbon stems [13]

The stems of *Alternanthera sessilis* was air dried and chopped into pieces of 2–5 cm length. It is carbonized in a muffle furnace at 750°C for 1 h under constant flow of nitrogen at 0.1 bar. The carbonized stem pieces were washed twice with double distilled water, followed by a single alcohol wash and finally dried in a hot air oven at 105°C for 24 h [13].

2.2.2. Synthesis of nano carbon particles

The carbonized stems of *Alternanthera sessilis* were soaked with waste engine oil for about 30 min and then air dried for about 1 h. The air dried, oil soaked carbonized stems were kept on a stainless steel grill and it is burnt from the bottom using LPG as fuel mixed with air as shown in Fig. 1. The soaked stems will start to burn at its ignition temperature, then the fuel gas (LPG) was cut off and the air inlet is regulated in such a way that, the combustion temperature was controlled at 420°C–470°C. The soot formed during the combustion was collected using a dome shaped surface of chromium oxide layer of stainless steel lid (316SS) which is kept over the combustion chamber (i.e., inside the catalytic surface). The excess flue gas was allowed to pass through the exhaust vents. The ash formed during the combustion process was frequently removed through the discharge opening provided at the bottom of the reactor. The carbon deposited at the inner surface of stainless steel dome was carefully collected and washed with double distilled water followed by alcohol.

2.3. Preparation of Y/Fe/TiO_2 sol

The Y and Fe co-doped TiO_2 photocatalyst was prepared by sol-gel process as per the following procedure. About 17 mL of ($Ti(OBu)_4$) was dissolved in 22 mL of ethanol with constant stirring and 1.5 mL of acetic acid was added drop-wise to suppress the hydrolysis. The above solution was stirred for 30 min using a magnetic stirrer to get the solution A. Solution B was prepared by adding 20 mL of 0.1 M $Y(NO)_3.6H_2O$ and 20 mL of 0.1 M $Fe(NO)_3$. Prepared solutions A and B were thoroughly mixed and the mixture was hydrolyzed at 25°C for about 30 min under agitation which yielded a transparent sol.

2.4. Preparation of Y/Fe/TiO_2@NCS

Exactly 0.5 g of NCS is stirred well with using a magnetic stirrer for about half an hour. To this suspension, transparent sol containing Y/Fe/TiO_2 was slowly added with constant stirring. After the addition of sol, the contents were stirred for 6 h and kept as such for further 24 h. After 24 h, the supernatant solution was decanted off and the contents were dried at 120°C until to get a solid mass. The solid composite was powdered well using mortar and pestle, and calcined for

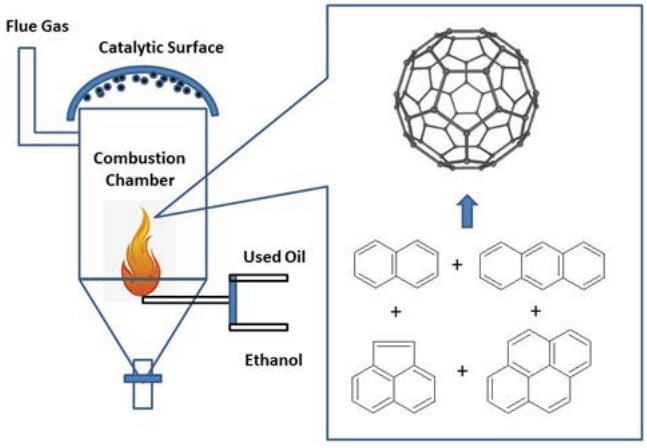

Fig. 1. Formation mechanism of NCS.

3 h at a temperature of 450°C under constant flow of N_2 gas. The powdered composite marked as Y/Fe/TiO_2@NCS and it was analyzed for its surface characteristics. This was used in the subsequent adsorption and photocatalytic studies.

2.5. Preparation of dye solution

A anionic dye – Direct Blue 71, with the molecular formula ($C_{40}H_{23}N_7Na_4O_{13}S_4$, MW: 1,029.87, C.I. No: 34,140 and λ_{max}: 594 nm, (E. Merck, India) was used in the photocatalytic degradation studies. In order to prepare a stock solution of Direct Blue 71 dye, an appropriate amount of solid dye (based on the percentage purity of the dye sample) was dissolved in double-distilled water. The stock solution was then used to prepare the diluted solutions as and when required. The structure of Direct Blue 71 is shown in Fig. 2.

2.6. Photocatalytic studies

The photocatalytic degradation study of the dye in an aqueous phase was done in an annular type photoreactor. This has a central lamp surrounded by 16 reaction cells. Light source is obtained from a high-pressure mercury vapor lamp (160 W, 210–240 V Philips India make) at the central axis. This generates UV radiation with a wavelength of $\lambda \geq 365$ nm. The reaction cells with a total capacity of 1,760 mL are made of Pyrex tubes. Similarly the photocatalysis under visible radiation was also carried out using a photoreactor made of tungsten filament lamp at the central axis surrounded by 16 reaction cells made up of borosilicate glass. During irradiation, the contents present in the reaction cells are continuously stirred using a magnetic stirrer.

Y/Fe/TiO_2@NCS photocatalyst of known quantity was added to 100 mL of Direct Blue 71 solution of particular concentration in the sampling tube. The temperature of the reaction was maintained at 30°C ± 3°C (room temperature) for all the experiments and the system was irradiated with a light source. For a particular time interval, the sample tube was removed from the slot, centrifuged using Universal (Make: India) centrifuge at 5,000 rpm for 5 min. Double beam UV–Vis spectrophotometer (Systronics, India, Model: 2201) was used to measure the final concentration of the dye solution by measuring the absorbance at the 594 nm (λ_{max} of Direct Blue 71 dye). The degradation studies repeated thrice and the largest deviation was 3% only.

2.7. Characterization studies

The scanning electron microscope (SEM) images were observed using QUANTA 250 FEG field emission scanning electron microscope. The X-ray diffraction (XRD) patterns were studied by X-ray diffractometer with Cu Kα radiation, operated at 40 kV and 30 mA. The high resolution transmission electron microscope (TEM) images were recorded using Jeol/JEM 2100 (Japan).

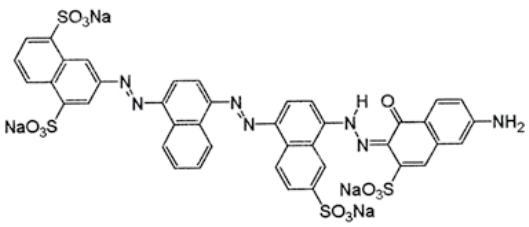

Fig. 2. Structure of Direct Blue 71 dye.

3. Results and discussion

3.1. NCS formation mechanism

The used motor oil contains 71% of base stock by weight, while the rest 29% are contaminants [14]. The lighter components of the lubricating oil get evaporated during operations owing to the higher temperature. Used motor oil typically contains long-chain hydrocarbons such as octane, hexane and substituted hexane. It also contains nearly 14% of sludge formed by the oxidative addition of long-chain hydrocarbons. High concentration of polycyclic aromatic hydrocarbons (PAH) such as naphthalene, acenaphthalene, anthracene, pyrene and substituted poly cyclic compounds were also found. The presence of these PAHs will favor the formation of fullerene-like carbon balls during the carbon formation. At higher temperature, this precursor oil decomposes and forms a carbon nucleus with solid/liquid and liquid/gas interfaces. These interfaces generally end with the radial and concentric texture growth of fluid cokes, which leads to the formation of NCS as shown in Fig. 3 [15].

3.2. Characteristics of NCS and Y/Fe/TiO_2@NCS

The prepared samples were analyzed with XRD to ascertain the various crystallographic planes and evaluated the crystal forms of the composite catalyst (Fig. 3). The XRD pattern of NCS has a broad peak at 25° which is generated due to the reflections of (002) graphitic plane. This is a typical pattern of amorphous structure with a d_{002} of 0.036 nm based on Bragg's equation (JCPDS 41-1487), which gives a quantitative measurement for the graphitic network [16]. Presence of another peak with low intensity is observed around 44° which is generated by the reflection of (100) graphitic plane [17]. The peaks pertaining to graphitic carbon are not present in the XRD pattern of the composite catalyst. However, a sharp and high intensity peak for the (101) plane of anatase form of titania is observed at 25.5°.

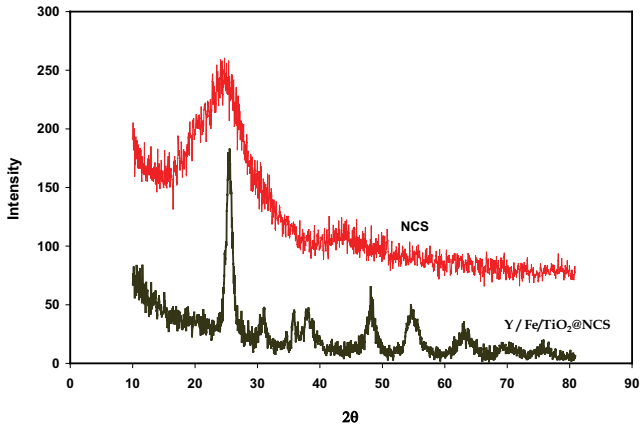

Fig. 3. XRD pattern of NCS and Y/Fe/TiO_2@NCS.

Other XRD peaks generated due to the reflections of (004) plane of anatase TiO_2 at 38.17°, peak at 48.12° for (200) plane of anatase TiO_2, peak at 54.57° for the (105) plane of anatase evidence the presence of doped titania on the NCS surface. The characteristic peaks for Fe_2O_3 are observed at a 2θ angles of 31.2° and 63.0° corresponding to the (206) and (4,0,12) planes, respectively (JCPDS card No. 25-1402) [18]. The doping of Y_2O_3 is proved (JCPDS 88 – 1040) by the XRD peaks at a 2θ values of 36.0°, 69.27° and 75.82° related to the reflections in (411), (800) and (811) planes, respectively [19].

The scanning electron microscopic images of NCS and Y/Fe/TiO_2@NCS are shown in Fig. 4. As observed from the SEM images of the pure carbon samples, the clusters of carbon nano spheres of sizes ranging between 50 and 80 nm are present. When the carbon is co-doped with Y/Fe/TiO_2, the composite grains are uniformly distributed over the surface of NCS.

The presence of elemental C and small amount of adsorbed oxygen in the energy dispersive X-ray spectroscopy (EDX) spectra (Fig. 5a) indicates that there are no impurities on its surface. In the case of the co-doped composite, the presence of Y, Fe and Ti over the surface of NCS is clearly shown in the EDX spectra (Fig. 5b). The SEM image indicates the surface topography and size distribution only. In order to find the hollowness as well as the crystalline nature of the NCS, the sample is subjected to TEM analysis. The TEM image of the NCS is presented in Fig. 6. From the TEM image Fig. 6a, the carbon spheres seem to be solid spheres. The other TEM image, Fig. 6b, indicates the presence of lattice fringes with about 4–5 graphitic layers in 2 nm range, which confirms the graphitic carbon having an interlayer distance of 0.4–0.6 nm [20]. The concentric layers with higher interlayer distances (compared with pure graphite) are due to the presence of gaseous molecules in between the graphitic layers [21]. The selected area diffraction pattern of a single carbon (Fig. 6c) is found to have concentric hollow circles which indicate highly disordered graphitic layers on the surface of carbon spheres [21].

The suitability and efficiency of a semiconductor photocatalyst purely depend on the energy gap between valence band and conduction band (i.e., the optical band gap). The optical band gap or direct band gap can be tailored with doping a different impurity atom [22,23]. It is reported that doping of yttrium with TiO_2 reduces the band gap to a considerable extent and shifts the absorption of light from UV to visible region [24]. The UV–DRS spectrum of the Y/Fe/TiO_2@NCS is shown in Fig. 7. Based on the UV–DRS studies, the calculated optical band gap for the composite catalyst is 2.73 eV. There is a considerable reduction in the band gap of the Y/Fe/TiO_2@NCS when compared with that of pure TiO_2 (3.2 eV). This reduction will bring the absorption wavelength of the Y/Fe/TiO_2@NCS well within the visible region. Further, the photocatalytic decomposition

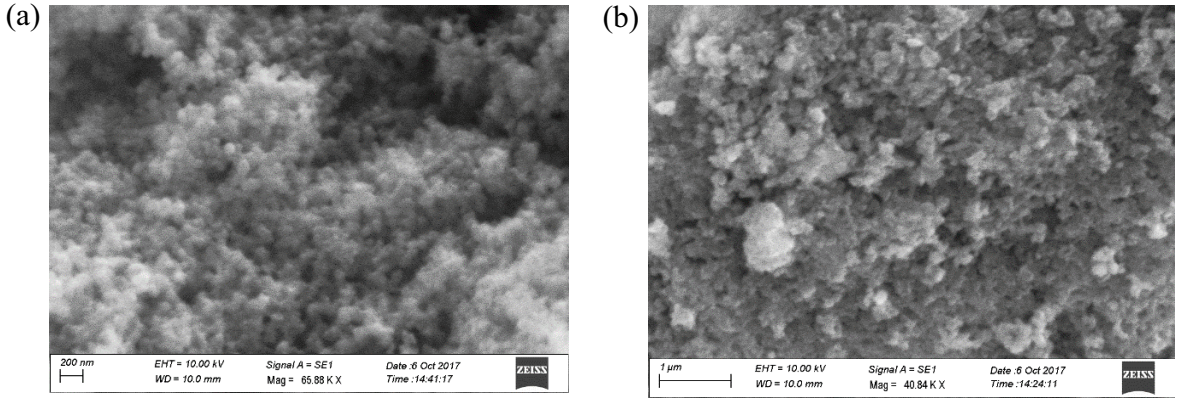

Fig. 4. SEM images (a) pure NCS and (b) Y/Fe/TiO_2@NCS.

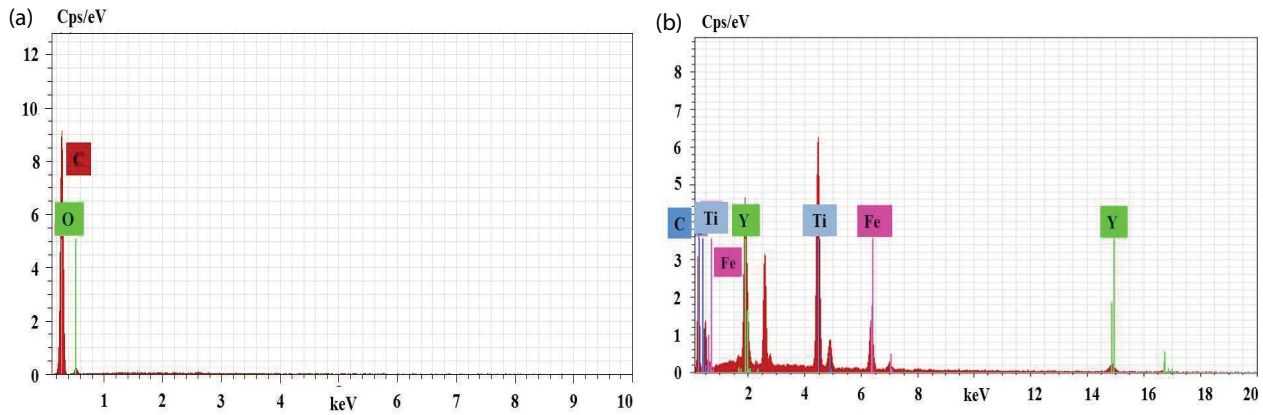

Fig. 5. EDX spectra (a) pure NCS and (b) Y/Fe/TiO_2@NCS.

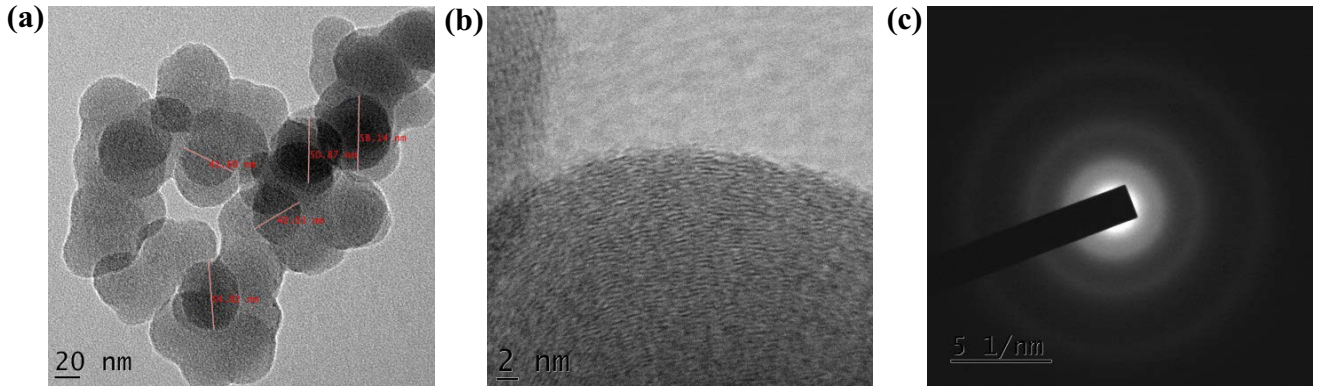

Fig. 6. TEM images NCS, (a) TEM image of the carbon sphere, (b) lattice fringes of NCS, and (c) selected area diffraction pattern of a single carbon.

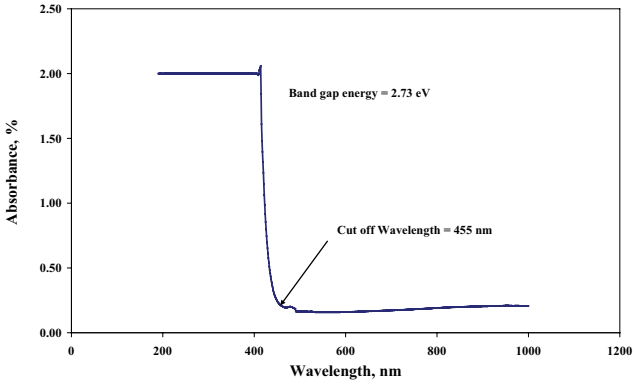

Fig. 7. Optical band gap analysis of Y/Fe/TiO_2@NCS.

ability of the Y/Fe/TiO_2@NCS is analyzed using the solar light and it is compared with the photodegradation under UV light in order to ascertain the suitability of the synthesized composite catalyst.

3.3. Photodegradation studies of DB71

The photocatalytic degradation of DB71 is evaluated under varying initial dye concentration from 50 to 200 mg/L. The dosage of the catalyst is fixed at 50 mg with a dye solution volume of 100 mL. Before analyzing the photocatalytic efficiency under UV and visible light, the dye solution is agitated under dark condition with the addition of the composite. As the host material for the composite catalyst is nano carbon, the carbon itself shows some adsorption. The maximum quantity of DB71 adsorbed onto the surface of carbon is 20.12% at an initial dye concentration of 50 mg/L and it decreases to 12.76% on increasing the dye concentration to 200 mg/L. Along with adsorption, a little amount of dye also degraded even in the absence of catalyst. The quantity of dye removed by photolysis is evaluated by exposing the dye solution under UV and solar light without any catalyst. Only a negligible amount of dye is degraded when the dye solution is exposed under the UV and solar light for 4 h. Hence, in this study, the dye degraded by direct photolysis is not considered.

The percentage variations in the dye (DB71) degradation at different concentrations under UV and solar light are shown in Figs. 8a and 8b, respectively. At an initial dye concentration of 50 mg/L, the catalyst is capable of degrading 100% dye molecules under UV as well as solar irradiations with an irradiation time of 60 min. On increasing the initial dye concentration from 50 to 200 mg/L, the maximum percentage of degradation decreased from 100% to 81.8% and 100% to 87.65% under UV and solar irradiations, respectively, with the same irradiation time. The catalyst is capable of degrading more dye molecules under visible light when compared with that of UV irradiation. This substantiated that high amount of electron–hole pair generated under the visible irradiation than UV light due to the reduction in the band gap. As the synthesized composite catalyst has a great activity under both UV as well as visible light, further degradation studies were performed under visible light only in order to achieve economy.

3.4. Effect of pH on DB71 degradation

The influence of solution pH on the degradation rate of any heterogeneous photocatalytic system is a highly complicated due to its complexity [25]. The complex organic dye molecules are fragmented by the hydroxyl radicals or directly oxidized by the positive holes or it can be reduced by the generated electron [25]. Among the above said three species, the actual species involved in the degradation process may vary depending upon the pH of the solution [26].

The electrical double layer generated at the solution–catalyst interface is greatly influenced by the pH of solution and pH_{zpc} of the catalyst. The double layer at the interface modifies the solute exposure on the catalyst surface and thereby alters the extent of degradation. The dye selected for the present study is an anionic azo dye which ionizes in aqueous solution as follows:

When the pH of solution is lower than pH_{zpc} of the catalyst, the catalyst surface has a positive charge which will attract the negatively charged dye species and hence the degradation rate is high. When the solution pH exceeds the pH_{zpc} of the catalyst, the surface of the catalyst acquires a negative charge which will not favor the adsorption of dye ions on the catalyst surface, thereby reduces the degradation rate. In the present system, the degradation of DB71 decreased from 94.0% to 93.0 % on increasing the solution pH from 2.0 to 7.0 (as shown in Fig. 9). When pH exceeds 7.0,

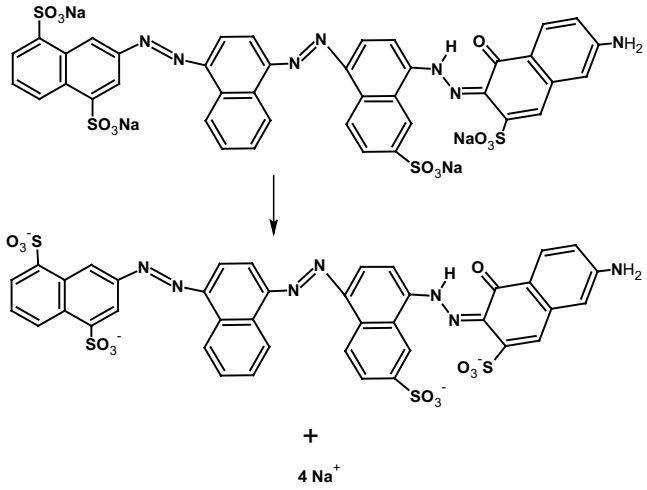

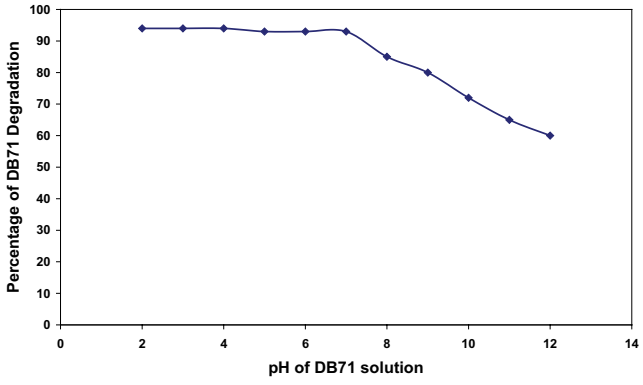

Fig. 9. Effect of DB71 solution pH on percentage degradation.

the degradation rate decreases and the degradation of DB71 decreases to 60.0% at a pH of 12.0.

3.5. Kinetics of DB71 degradation

In-order to evaluate the real mechanism of photodegradation as well as the number of molecules which actually determines the degradation rate, the kinetic data were analyzed using the linear and non-linear first-order kinetic equation. The first-order rate constant was calculated from the slope of the linearized plot of $\ln\frac{C_0}{C_t}$ vs. time (figure not shown). The first-order rate constant calculated from the linear plot decreased from 0.0784 to 0.0329 on increasing the concentration from 50 to 200 mg/L of DB71 (Table 1). The linear plot has a correlation coefficient value of $0.9538 < r^2 < 0.9963$. The experimental data fit well with the first-order kinetics model for the degradation of DB71 by Y/Fe/TiO_2@NCS.

According to Lima et al. [27], linearizing the mathematical models will lead to error in the calculated results. Therefore, in this study, in-order to evaluate the extent of error raised from the linear model, the kinetic data were analyzed using non-linear curve fitting model with the help of MS Excel data solver tool. In the non-linear analysis of the kinetic data, the standard deviation between the experimental C_t and the C_t calculated using the non-linear first-order kinetic equation is estimated. The non-linear curve is made to match with the experimental C_t by setting a goal to minimize the square of standard deviation. The variables set are k_{app} and n, the calculated values are presented in Table 2. Where k_{app} is the apparent rate constant of first-order decomposition of DB71 and n is the order of decomposition.

In the analysis, the variables k_{app} and n are optimized by setting minimum standard deviation as the goal. On increasing the initial DB71 concentration from 50 to 200 mg/L, the order of photodecomposition increased from 1.5439 to 2.3266, which indicates that the decomposition of DB71 by Y/Fe/TiO_2@NCS is not a pure first order [28]. The order is more than one and the order of DB71 decomposition increases with concentration. The decomposed products ($[DB]_f$) also acted as reactants and this led the reaction into higher order. Initially the decomposition of dye in the preliminary stage depended on the intensity of light radiation as well as the concentration of undissociated dye molecules [29]. This can be represented as follows:

$$[\mathrm{DB71}] \xrightarrow{h\gamma} [\mathrm{DB71}]_f \qquad \text{(I)}$$

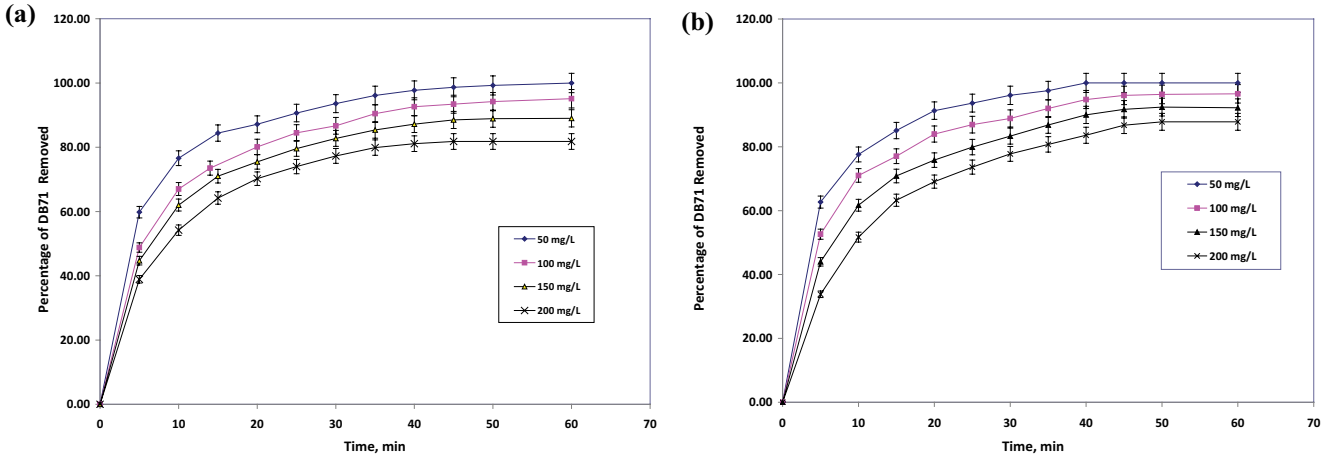

Fig. 8. Degradation of DB71 (a) under UV light and (b) under solar light.

Table 1
Results of linear first-order and L-H plots

First-order linear plot results			L-H plot		
Initial DB71 concentration, mg/L	k_{app}	r^2	K_r	K	r^2
50	0.0784	0.9832	0.145	226.42	0.8717
100	0.063	0.9963			
150	0.0431	0.9798			
200	0.0329	0.9538			

Table 2
Results of non-linear first-order kinetic studies

S. No	Concentration of DB71 (mg/L)	n	k_{app}	S_d
1	50	1.5439	0.0267	2.60
2	100	1.7181	0.0060	3.37
3	150	2.0217	0.0010	3.24
4	200	2.3174	0.0001	2.16

$$\text{The rate of DB71 decomposition} \propto \left[\text{DB71}\right] \quad \text{or}$$
$$= k_i \left[\text{DB71}\right] \tag{1}$$

where k_i is the rate constant in the preliminary stage of photodecomposition of the dye. At this beginning stage the order of the reaction is unity. $[DB71]_f$ is the concentration of DB71 dye fragments at higher concentrations and on the latter stage of the reaction [30]. Under these circumstances, the rate of the photodecomposition of the dye can be denoted as follows:

$$\text{The rate of decomposition} \propto \left[\text{DB71}\right] \times \left[\text{DB71}\right]_f$$
$$= k\left[\text{DB71}\right] \times \left[\text{DBH}\right]_f \tag{2}$$

The order of the photodecomposition is more than one and it is 2.3266 at 200 mg/L of DB71 under higher concentration. The non-linear analyses proved that the order of photodecomposition of DB71 by Y/Fe/TiO_2@NCS is more than one. As the fractional orders cannot be determined using linearized kinetic models, in such context, the non-linear kinetic model suited best for the evaluation of the rate of degradation by the selected catalyst.

3.6. Analysis of Langmuir–Hinshelwood model

The Langmuir–Hinshelwood kinetic model is also one of the models to describe the kinetics of heterogeneous photocatalytic system [31]. In the present study, the L-H-kinetic model is used without approximating it to first-order kinetic expression. The approximation of L-H model to first-order kinetics is not correct for the estimation of L-H model parameters.

The L-H kinetic expression is given by:

$$r_0 = \frac{-dc}{dt} = \frac{K_r K C_0}{1 + K C_0} \tag{3}$$

where K_r is the limiting rate constant of reaction at maximum coverage and K is the adsorption equilibrium constant. From the L-H kinetic model plot (figure not shown), the plot of $1/r_0$ Vs. $1/C_0$ for the photo-induced decomposition of DB71 by Y/Fe/TiO_2@NCS, a linear variation was observed. The liner variation of L-H plot for the DB71 decomposition confirmed the Langmuir–Hinshelwood relationship to the initial rate of DB71 photodegradation by Y/Fe/TiO_2@NCS [32]. The values of K_r and K calculated from the slope and intercept of the L-H plot are presented in Table 1. The limiting rate constant of reaction at maximum coverage K_r was 0.145 and another constant found to have 226.42 with a correlation coefficient of 0.8717.

4. Conclusion

Waste engine oil is used as precursor for the synthesis of NCS in the range of 50–80 nm. The multi-metal catalyst prepared using the ash of *Alternanthera sessilis* stem helped the formation of carbon balls. Y/Fe/TiO_2 is co-doped onto NCS for the preparation of composite catalyst. The XRD, SEM, EDX, TEM and UV–DRS analyses were helpful for the characterization of the composite catalyst. The TEM image proved the presence of lattice fringes with about 4–5 graphitic layers in 2 nm range, which confirmed the graphitic carbon having an interlayer distance of 0.4–0.6 nm. The band gap of TiO_2 is decreased from 3.2 to 2.73 eV, and showed a considerable reduction in the co-doped carbon composite. The composite catalyst, therefore, had great potential for the removal of direct blue 71 dye under UV as well as solar irradiations. The non-linear analyses proved that the order of photodecomposition of DB71 by Y/Fe/TiO_2@NCS under visible light is more than one.

Acknowledgment

The author Dr. P. Sivakumar would like to thank the University Grants Commission (UGC), Hyderabad, India, for the financial assistance under "Minor Research Project Scheme" (Project Ref.: F MRP-6449/16 (SERO/UGC), Link No: 6449, Dt: 03.06.2017).

References

[1] The World Population Prospects: The 2017 Revision, UN Department of Economic and Social Affairs, United Nations, New York, 2017.
[2] M. Khan, W. Cao, M. Ullah, *Ab initio* calculations for the electronic and optical properties of Y-doped anatase TiO_2, Phys. Status Solidi B, 250 (2013) 364–369.
[3] J. He, Q. Liu, Z. Sun, W. Yan, G. Zhang, Z. Qi, P. Xu, Z. Wu, S. Wei, High photocatalytic activity of rutile TiO_2 induced by iodine doping, J. Phys. Chem. C, 114 (2010) 6035–6038.
[4] M. Li, J. Zhang, Y. Zhang, First-principles calculation of compensated (2N, W) codoping impacts on band gap engineering in anatase TiO_2, Chem. Phys. Lett., 527 (2012) 63–66.
[5] J. Lu, Y. Dai, M. Guo, L. Yu, K. Lai, B. Huang, Chemical and optical properties of carbon-doped TiO_2: a density-functional study, Appl. Phys. Lett., 100 (2012) 102114.
[6] M. Khan, J. Xu, N. Chen, W. Cao, First principle calculations of the electronic and optical properties of pure and (Mo, N) co-doped anatase TiO_2, J. Alloys Compd., 513 (2012) 539–545.

[7] A.-W. Xu, Y. Gao, H.-Q. Liu, The preparation, characterization, and their photocatalytic activities of rare-earth-doped TiO_2 nanoparticles, J. Catal., 207 (2002) 151–157.
[8] C. Liang, C. Liu, F. Li, F. Wu, The effect of praseodymium on the adsorption and photocatalytic degradation of azo dye in aqueous Pr^{3+}-TiO_2 suspension, Chem. Eng. J., 147 (2009) 219–225.
[9] C.J. Kim, H.H. Choi, C.H. Sohn, Auto-ignition of lubricating oil working at high pressures in a compressor for an air conditioner, J. Hazard. Mater., 161 (2009) 416–422.
[10] W. Smith, S. Mao, G. Lu, A. Catlett, J. Chen, Y. Zhao, The effect of Ag nanoparticle loading on the photocatalytic activity of TiO_2 nanorod arrays, Chem. Phys. Lett., 485 (2010) 171–175.
[11] C.M. Fan, P. Xue, Y.P. Sun, Preparation of nano-TiO_2 doped with cerium and its photocatalytic activity, J. Rare Earths, 24 (2006) 309–313.
[12] Y. Wang, K. Lu, C. Feng, Photocatalytic degradation of methyl orange by polyoxometalates supported on yttrium-doped TiO_2, J. Rare Earths, 29 (2011) 866–871.
[13] B. Murugesan, A. Sivakumar, A. Loganathan, P. Sivakumar, Synthesis and photocatalytic studies of lanthanum oxide doped nano carbon hollow spheres, J. Taiwan Inst. Chem. Eng., 71 (2017) 364–372.
[14] V.A. Litvishkova, A.I. Bukhter, A.V. Nepogod'ev, A.M. Bezhanidze, Chemical composition of used motor oils, Chem. Technol. Fuels Oils, 10 (1974) 962–965.
[15] M. Inagaki, Discussion of the formation of nanometric texture in spherical carbon bodies, Carbon, 35 (1997) 711–713.
[16] S.H. Ng, J. Wang, Z.P. Guo, J. Chen, G.X. Wang, H.K. Liu, Single wall carbon nanotube paper as anode for lithium-ion battery, Electrochim. Acta, 51 (2005) 23–28.
[17] A. Nieto-Marquez, I. Espartero, J.C. Lazo, A. Romero, J.L. Valverde, Direct synthesis of carbon and nitrogen–carbon nanospheres from aromatic hydrocarbons, Chem. Eng. J., 153 (2009) 211–216.
[18] J. Huang, S. Yang, Y. Xu, X. Zhou, X. Jiang, N. Shi, D. Cao, J. Yin, G. Wang, Fe_2O_3 sheets grown on nickel foam as electrode material for electrochemical capacitors, J. Electroanal. Chem., 713 (2014) 98–102.
[19] H. Wang, C. Qian, Z. Yi, L. Rao, H. Liu, S. Zeng, Hydrothermal synthesis and tunable multicolor upconversion emission of cubic phase Y_2O_3 nanoparticles, Adv. Condens. Matter Phys., 2013 (2013) 1–6.
[20] K.S. Kumar, C.-G. Song, G.M. Bak, G. Heo, M.-J. Seong, J.-W. Yoon, Phase control of yttrium (Y)-doped TiO_2 nanofibers and intensive visible photoluminescence, J. Alloys Compd., 617 (2014) 683–687.
[21] G.M. Yang, Q. Xu, H.W. Tian, X. Wang, W.T. Zheng, Amorphous hollow carbon spheres synthesized using radio frequency plasma-enhanced chemical vapour deposition, J. Phys. D: Appl. Phys., 41 (2008) 195504.
[22] L. Chiodo, J.M. Garcia-Lastra, A. Iacomino, S. Ossicini, J. Zhao, H. Petek, A. Rubio, Self-energy and excitonic effects in the electronic and optical properties of TiO_2 crystalline phases, Phys. Rev. B: Condens. Matter, 82 (2010) 045207.
[23] W. Kang, M.S. Hybertsen, Quasiparticle and optical properties of rutile and anatase TiO_2, Phys. Rev. B: Condens. Matter, 82 (2010) 085203.
[24] X. Niu, S. Li, H. Chu, J. Zhou, Preparation, characterization of Y^{3+}-doped TiO_2 nanoparticles and their photocatalytic activities for methyl orange degradation, J. Rare Earths, 29 (2011) 225–229.
[25] K.M. Reza, A.S.W. Kurny, F. Gulshan, Parameters affecting the photocatalytic degradation of dyes using TiO_2: a review, Appl. Water Sci., 7 (2017) 1569–1578.
[26] W.Z. Tang, Z. Zhang, H. An, M.O. Quintana, D.F. Torres, TiO_2/UV photodegradation of azo dyes in aqueous solutions, Environ. Technol., 18 (1997) 1–12.
[27] E.C. Lima, M.A. Adebayo, F.M. Machado, Kinetic and Equilibrium Models of Adsorption, Chapter 3, C.P. Bergmann, F.M. Machado Eds., Carbon Nanomaterials as Adsorbents for Environmental and Biological Applications, Springer, 2015, pp. 33–69.
[28] S.Y. Lou, X.B. Jia, Y.Q. Wang, S.M. Zhou, Template-assisted in-situ synthesis of porous AgBr/Ag composite microspheres as highly efficient visible-light photocatalyst, Appl. Catal., B, 586 (2015) 176–177.
[29] R. Kopelman, Fractal reaction kinetics, Science, 241 (1988) 1620–1626.
[30] C. Wang, Fractional kinetics of photocatalytic degradation, J. Adv. Dielectr., 8 (2018) 1850034.
[31] K. Vasanth Kumar, K. Porkodi, A. Selvaganapathi, Constrain in solving Langmuir–Hinshelwood kinetic expression for the photocatalytic degradation of Auramine O aqueous solutions by ZnO catalyst, Dyes Pigm., 75 (2007) 246–249.
[32] S. Rahnamaeiyan, S. Khademolhoseini, Preparation and characterization of cadmium titanate nanoparticles via novel sol–gel method and its photocatalyst application, J. Mater. Sci. - Mater. Electron., 27 (2016) 6043–6047.